Generalized Finite Difference Method for Numerical Solutions of Density-driven Groundwater Flows

Po-Wei Li[1]**, Chia-Ming Fan**[1,2]**, Chun-Yu Chen**[1] **and Cheng-Yu Ku**[1]

Abstract: A combination of the generalized finite difference method (GFDM), the implicit Euler method and the Newton-Raphson method is proposed to efficiently and accurately analyze the density-driven groundwater flows. In groundwater hydraulics, the problems of density-driven groundwater flows are usually difficult to be solved, since the mathematical descriptions are a system of time- and space-dependent nonlinear partial differential equations. In the proposed numerical scheme, the GFDM and the implicit Euler method were adopted for spatial and temporal discretizations of governing equations. The GFDM is a newly-developed meshless method and is truly free from time-consuming mesh generation and numerical quadrature. Based on the concept of star in the GFDM and the moving-least-squares method, the derivatives with respect to space coordinates at every node are expressed by linear combinations of nearby function values with different weighting coefficients. After discretizations of the GFDM and the implicit Euler method, a system of nonlinear algebraic equations at every time step is yielded and then can be efficiently solved by the Newton-Raphson method. Two numerical tests including the Henry and the Elder problems were adopted to verify the accuracy and the stability of the proposed meshless numerical scheme. Besides, the numerical results were compared with other numerical and semi-analytical solutions.

Keywords: Meshless numerical scheme, density-driven groundwater flow, generalized finite difference method, Newton-Raphson method, Henry and Elder problems.

1 Introduction

The study of density-driven groundwater flows is one important branch in groundwater hydraulics, since they are related to problems of saltwater intrusion and

---

[1] Department of Harbor and River Engineering & Computation and Simulation Center, National Taiwan Ocean University, Keelung 20224, Taiwan.

[2] Corresponding Author. E-mail: cmfan@ntou.edu.tw

geothermal processes. In coastal states, encircled by oceans, freshwater resource is extremely important and precious. In some areas, groundwater resource has been frequently used to supply freshwater to livelihood of people; therefore, the problems of seawater intrusion to groundwater at the coastal areas are very essential and should be paid more attention. In the past, many researchers have focused on the problems of density-driven groundwater flows. From their study and experiences, there are two standard numerical tests of the density-driven groundwater flows, which include the Henry problem [Gotovac, Andricevic, Gotovac, Kozulic and Vranjes (2003); Henry (1964); Pinder and Cooper Jr. (1970); Segol, Pinder and Gray (1975); Simpson and Clement (2004)] and the Elder problem [Elder (1967); Simpson and Clement (2003)]. The Henry problem is commonly adopted to discuss the transmission of salt concentration in freshwater by fluid flow, that plays an important role to coastal nations. On the other hand, the Elder problem is used for describing free geothermal convection problems.

The Henry problem is named after Henry (1964) studied problems of transmission of salt concentration and developed a semi-analytical solution of the steady-state salt concentration in a confined coast aquifer. Pinder and Cooper Jr. (1970) acquired a transient semi-analytical solution of the Henry problem by using the method of characteristics, as Segol, Pinder and Gray (1975) used the Galerkin finite element method to numerically study the Henry problem. On the other hand, the Elder problem is named after the study of Elder (1967). Elder (1967) studied a heat-driven convection problem in a two-dimensional cross-section and used a Hele-Shaw cell to verify his results. Later, Simpson and Clement (2003) numerically found that the Elder problem is highly sensitive to discretization. From the above discussions, it can be deduced that it is non-trivial to develop an efficient, accurate, reliable and simple numerical scheme to study the Henry problem and the Elder problem.

According to the Darcy's law, the principles of mass conservation and solute transport, and the Boussineq approximation, the mathematical descriptions of the density-driven groundwater flows are highly nonlinear and very complicated. Thus, many numerical methods have been proposed to analyze these problems. For example, Soto Meca, Alhama and Gonzalez Fernandez (2007) proposed a numerical model based on the network simulation method to analyze two-dimensional problems of density-driven groundwater flows, while Kovarik and Muzik (2013) applied the local boundary integral method and the radial basis function approximation to analyze the Henry and the Elder problems. In both of their researches, the numerical results are very similar to the solutions from other studies [Gotovac, Andricevic, Gotovac, Kozulic and Vranjes (2003); Simpson and Clement (2003); Simpson and Clement (2004)]. Although many numerical schemes have been proposed to ana-

lyze the problems of density-driven groundwater flows, it is still important to develop a simple, reliable, accurate, efficient and stable numerical method. Hence, in this paper, we adopted a newly-developed meshless numerical method to efficiently and accurately analyze the Henry and the Elder problems.

With the rapid developments of computer technology, many numerical methods have been developed for numerical solutions of various engineering problems. The numerical methods for spatial discretizations of partial differential equations can be roughly classified as mesh-dependent and meshless (or meshfree) methods. By comparing with mesh-dependent methods, the numerical implementations of meshless methods are simple the numerical results are much accurate, since to use the meshless methods can avoid dealing with time-consuming mesh generation and numerical quadrature. As far as the meshless methods are concerned, they can be divided into two groups: boundary-type methods and domain-type methods. The method of fundamental solutions [Gaspar (2013); Liu and Sarler (2013); Tsai and Young (2013)], the boundary knot method [Lin, Chen, Chen, Jiang (2013); Zheng, Chen and Zhang (2013)], the Trefftz method [Fan, Li, Hsu and Lin (2014); Fan, Liu, Chan and Hsiao (2014)] and the singular boundary method [Chen, Fu and Wei (2009)] are four of the most-promising boundary-type meshless methods, since only boundary nodes are necessary during numerical simulations. Although dimensionality of considered problems can be reduced by one, these methods can be adopted only for numerical solutions of homogeneous partial differential equations. Once inhomogeneous partial differential equations are considered, the above-mentioned boundary-type meshless methods have to cooperate with other domain-type methods.

In contrast to the boundary-type methods, the domain-type meshless methods without any cooperation can directly analyze inhomogeneous partial differential equations since both of boundary nodes and interior nodes are used during implementations. The method of approximate particular solutions [Chen, Fan and Wen (2011); Chen, Fan and Wen (2012)], the local radial basis function collocation method [Chan and Fan (2013); Fan, Chien, Chan and Chiu (2013); Mramor, Vertnik and Sarler (2013)], the generalized finite difference method (GFDM) [Benito, Urena and Gavete (2001); Benito, Urena and Gavete (2007); Benito, Urena, Gavete and Alonso (2008); Chan, Fan and Kuo (2013); Fan, Huang, Li and Chiu (2014); Gavete, Urena and Benito (2003); Gavete, Urena, Benito and Gavete (2012); Urena, Benito and Gavete (2011)] and the meshless local Petrov-Galerkin method [Mirzaei and Dehghan (2011); Sladek, Sladek, Krahulec, Wunsche and Zhang (2012)] are four of the newly-developed domain-type meshless methods. The above-mentioned four domain-type meshless methods can be adopted for numerical solutions of various partial differential equations. The advantages and disadvantages of these meth-

ods as well as potential engineering applications are worthy to be investigated further.

Among them, the GFDM is one of the most-promising domain-type meshless methods. According to the moving-least-squares method, the derivatives with respect to space coordinates can be expressed as linear combinations of nearby function values within a star. By comparing with classical finite difference method, the GFDM can use non-uniform grids and be easily applied to problems in irregular computational domain. The GFDM remains the merits of the classical finite difference method, such as the simplicity and wide applicability to various engineering problems, since it is evolved from the classical finite difference method. Benito, Urena and Gavete (2001) proposed the explicit numerical procedure of the GFDM and examined several factors of the GFDM. Then, Benito, Urena and Gavete (2007) applied the GFDM to parabolic and hyperbolic partial differential equations, while Benito, Urena, Gavete and Alonso (2008) proposed an *h*-adaptive method for the GFDM for numerical solutions of second-order partial differential equations with constant coefficients. Chan, Fan and Kuo (2013) adopted the GFDM with the fictitious time integration method (FTIM) for solving two-dimensional nonlinear obstacle problems, as Fan, Huang, Li and Chiu (2014) used the GFDM to stably solve the inverse biharmonic boundary-value problems without any well-known regularization method. From the brief discussions of the GFDM, we can find that the GFDM is a newly-developed meshless method and only has been adopted for numerical solutions of simple partial differential equations. Since the GFDM has great potential to be extended to various engineering problems, we adopted the GFDM for spatial discretization of the governing equations of density-driven groundwater flows. In this paper, it is the first time that the GFDM is adopted for numerical solutions of system of nonlinear, coupled, time- and space-dependent partial differential equations.

For the two-dimensional problems of density-driven groundwater flows, the governing equations of the Henry and the Elder problems are systems of time- and space-dependent non-linear partial differential equations. The GFDM and the implicit Euler method were adopted for spatial and temporal discretizations of the governing equations. To adopt the implicit Euler method can acquire better stability of numerical simulation in comparison with the explicit Euler method. After these discretizations, a system of nonlinear algebraic equations is yielded and then is efficiently solved by the Newton-Raphson method. Recently, some novel solvers for system of nonlinear algebraic equations have been developed, such as the FTIM [Liu and Atluri (2008); Liu and Atluri (2009)] and the scalar homotopy method (SHM) [Fan, Liu, Yeih and Chan (2010)]. Though in some cases the FTIM and the SHM outperform the Newton-Raphson method, some free parameters in the FTIM

and the SHM should be determined manually and are needed more investigations. Thus, we adopted the Newton-Raphson method in our study to form a stable and reliable numerical scheme to study the problem of density-driven groundwater flows. In the Newton-Raphson method, the original formula for iteration is split into two sequent steps in order to avoid the time-consuming calculation of inverse of Jacobian matrix. In the first step, a sparse system of linear algebraic equations can be efficiently solved since the Jacobian matrix in the proposed numerical scheme is sparse. Then values at the new iteration step can be acquired by simple addition. Therefore, the main objective of the present study is to develop a simple, efficient and accurate numerical scheme in order to study the problems of density-driven groundwater flows. A combination of the GFDM, the implicit Euler method and the Newton-Raphson method was proposed for numerical solutions of density-driven groundwater flows in this paper. Two benchmark problems, the Henry and the Elder problems, were numerically examined. In addition, the numerical results were compared with other numerical and semi-analytical solutions to verify the accuracy and the stability of the proposed numerical scheme.

The motivation of this study and the discussions of relevant literatures are provided in the first section. Then, the mathematical descriptions of the Henry and the Elder problems as well as the numerical procedures of the proposed method are described. Followings are some numerical results and comparisons. Finally, conclusions and discussions are drawn.

2   Governing equations

According to previous researches, there are two benchmark problems of the densitydriven groundwater flows, the Henry problem and the Elder problem. The main differences between these two problems are the mechanism for transmission of salt concentration. In the Henry problem, the salt concentration is transported by fluid flow. By contrast, the salt concentration in the Elder problem is only transported by variation of fluid density. The governing equations, boundary conditions and initial conditions for these two problems are described in the following subsections.

2.1   *Henry problem*

The computational domain of the Henry problem is a vertical section of uniform, isotropic rectangular aquifer which initially enriched freshwater, and is shown in Fig. 1(a). According to the Darcy's law, mass conservation equation, salt transport equation and the Boussineq approximation, the governing equations of the Henry
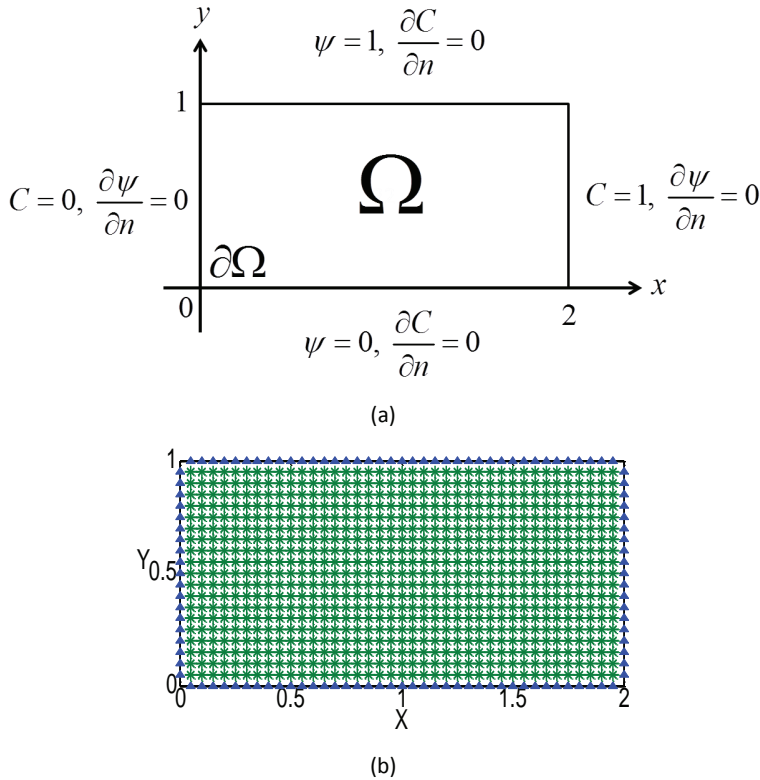
Figure 1: (a) The schematic diagram and (b) the distribution of nodes for the Henry problem.

problem have been derived,

$$\frac{\partial^2 \psi}{\partial x^2} + \frac{\partial^2 \psi}{\partial y^2} = \frac{1}{a}\frac{\partial c}{\partial x}, \tag{1}$$

$$\frac{\partial^2 c}{\partial x^2} + \frac{\partial^2 c}{\partial y^2} - \frac{1}{b}\left(\frac{\partial \psi}{\partial y}\frac{\partial c}{\partial x} - \frac{\partial \psi}{\partial x}\frac{\partial c}{\partial y}\right) = \frac{\partial c}{\partial t}, \tag{2}$$

where $c(x,y,t)$ is the salt concentration and $\psi(x,y,t)$ is the streamfunction. a and b are the discharge parameter and the inverse of seepage Peclet number, respectively. x and y are spatial coordinates as well as t is the time. These variables are dimensionless and the readers, who are interested in detailed derivations of the governing equations, can refer to Gotovac, Andricevic, Gotovac, Kozulic and Vranjes (2003). This aquifer is initially filled with still freshwater, such that the initial conditions

for streamfunction and concentration are $\psi(x,y,t=0)=0$ and $c(x,y,t=0)=0$. The top and the bottom boundary are impermeable and a constant inflow is imposed along the left vertical boundary. The vertical right-side boundary is assumed to be the seaside boundary and the dimensionless concentration $c(x=2,y,t)=1$ is imposed. The boundary conditions for streamfunction and salt concentration are demonstrated in Fig. 1(a).

2.2 Elder problem

The computational domain of the Elder problem is also a rectangular two-dimensional domain with a homogeneous isotropic porous medium. The saltwater source is specified along middle half of the top boundary, while the bottom boundary is maintained at zero concentration which is shown in Fig. 2(a). The dimensionless form of mathematical descriptions for the Elder problem is expressed as follows [Soto Meca, Alhama and Gonzalez Fernandez (2007)]

$$\frac{\partial^2 \psi}{\partial x^2} + \frac{\partial^2 \psi}{\partial y^2} = Ra\frac{\partial c}{\partial x}, \tag{3}$$

$$\frac{\partial^2 c}{\partial x^2} + \frac{\partial^2 c}{\partial y^2} - \left(\frac{\partial \psi}{\partial y}\frac{\partial c}{\partial x} - \frac{\partial \psi}{\partial x}\frac{\partial c}{\partial y} \right) = \frac{\partial c}{\partial t}, \tag{4}$$

where Ra is the Rayleigh number which is a dimensionless parameter. The initial conditions is the same as the Henry problem, $\psi(x,y,0)=0$ and $c(x,y,0)=0$. The boundary condition for streamfunction is zero along four sides of whole boundary, which means no inflow and outflow along any segment of boundary. The detailed descriptions of boundary conditions for streamfunction and salt concentration are depicted in Fig. 2(a).

3 Numerical methods

Although the mechanism for groundwater flows in the Henry problem and the Elder problem is quite different, the governing equations for these two problems are similar to each other. In this paper, we proposed a combination of the GFDM, the implicit Euler method and the Newton-Raphson method for numerical solutions of density-driven groundwater flows. The GFDM and the implicit Euler method are adopted for spatial and temporal discretizations, respectively. Then, a system of nonlinear algebraic equations at every time step is yielded and then solved by the Newton-Raphson method. The descriptions of these methods are given in the following subsections.
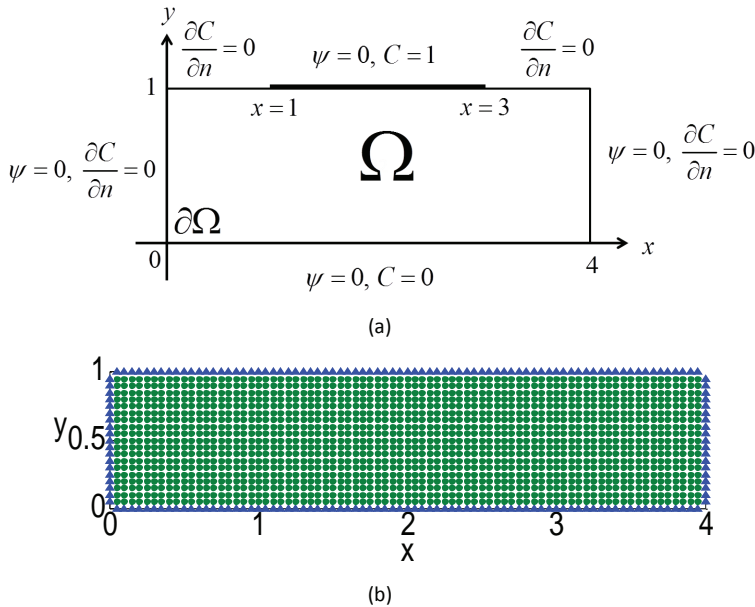
Figure 2: (a) The schematic diagram and (b) the distribution of nodes for the Elder problem.

3.1 Implicit Euler method

When the implicit Euler method is adopted for temporal discretization of governing equations, every term in equations belong to the $(n+1)^{th}$ time step and the time derivative is discretized by the forward difference scheme. The variables at the nth time step are known while the variables at the $(n+1)^{th}$ time step are unknowns. The governing equations of the Henry problem are discretized

$$\frac{\partial^2 \psi^{n+1}}{\partial x^2} + \frac{\partial^2 \psi^{n+1}}{\partial y^2} = \frac{1}{a}\frac{\partial c^{n+1}}{\partial x}, \tag{5}$$

$$\frac{\partial^2 c^{n+1}}{\partial x^2} + \frac{\partial^2 c^{n+1}}{\partial y^2} - \frac{1}{b}\left(\frac{\partial \psi^{n+1}}{\partial y}\frac{\partial c^{n+1}}{\partial x} - \frac{\partial \psi^{n+1}}{\partial x}\frac{\partial c^{n+1}}{\partial y}\right) = \frac{c^{n+1} - c^n}{\Delta t}, \tag{6}$$

where Δt is time increment. The superscripts n and $n+1$ denote the variables at the nth and the $(n+1)^{th}$ time steps. In addition, the governing equations for the Elder problem are expressed as,

$$\frac{\partial^2 \psi^{n+1}}{\partial x^2} + \frac{\partial^2 \psi^{n+1}}{\partial y^2} = Ra\frac{\partial c^{n+1}}{\partial x}, \tag{7}$$

$$\frac{\partial^2 c^{n+1}}{\partial x^2} + \frac{\partial^2 c^{n+1}}{\partial y^2} - \left(\frac{\partial \psi^{n+1}}{\partial y} \frac{\partial c^{n+1}}{\partial x} - \frac{\partial \psi^{n+1}}{\partial x} \frac{\partial c^{n+1}}{\partial y} \right) = \frac{c^{n+1} - c^n}{\Delta t}. \tag{8}$$

Since the implicit Euler method was used for time discretizations in the Henry problem and the Elder problem, the resultant governing equations for both problems become time-independent systems of nonlinear partial differential equations for the variables at the $(n+1)^{th}$ time step. Then, the GFDM was used for spatial discretizations for the above two systems.

3.2 Generalized finite difference method

In order to accurately and efficiently solve the problems of density-driven groundwater flows, the GFDM was applied for spatial discretizations of the governing equations and the boundary conditions. The GFDM is based on the moving-least-squares method to approximate the derivatives at every point in computational domain, such that the derivatives can be expressed by linear summations of nearby function values with different weighting coefficients.

When a given i^{th} node is considered, n_s nearest nodes around the ith node can be determined to form a star. For simplicity, a circular star is used in this paper, although in previous study [Benito, Urena and Gavete (2001)] various choices for the shapes of star have been proposed. There is an optimal choice for n_s depending on the required accuracy and the available computer power, since more accurate results can be acquired by using more nodes in a star. Based on our experience in adopting the GFDM [Chan, Fan and Kuo (2013); Fan, Huang, Li and Chiu (2014)], satisfying numerical results can be stably acquired while n_s is larger than 10 for practical computations. Consequently, in the numerical experiments of this paper, n_s is larger than 10.

Once the star for the ith node is formed, we use Taylor series to expand the function inside the star and then a new functional, $B(u)$, can be defined. Let u_i be the function value at the central i^{th} node of the star with coordinates (x_i, y_i) and $u_{i,j}(j = 1, 2, 3, \cdots, n_s)$ denote the values at the other nodes inside the star with coordinates $(x_{i,j}, y_{i,j})$. Defining a functional [Benito, Urena and Gavete (2001)]:

$$B(u) = \sum_{j=1}^{n_s} \left[\left(u_i - u_{i,j} + h_{ij} \frac{\partial u_i}{\partial x} + k_{ij} \frac{\partial u_i}{\partial y} + \frac{1}{2} \left(h_{ij}^2 \frac{\partial^2 u_i}{\partial x^2} + k_{ij}^2 \frac{\partial^2 u_i}{\partial y^2} + 2 h_{ij} k_{ij} \frac{\partial^2 u_i}{\partial x \partial y} \right) \right) w(h_{ij}, k_{ij}) \right]^2, \tag{9}$$

where j is the local index in the star. $h_{ij} = x_i - x_{i,j}$ and $k_{ij} = y_i - y_{i,j}$ are the distances between the ith node and the jth node along x and y directions and $w(h_{ij}, k_{ij})$ is the weighting function at $(x_{i,j}, y_{i,j})$. There are some choices of the weighting functions [Benito, Urena and Gavete (2001)], such as potential function, cubic

spline and quartic spline. Acceptable results can be obtained by using anyone of the above-mentioned weighting functions. Thus, the quartic spline was adopted as the weighting function in this paper:

$$w(d_{ij}) = \begin{cases} 1 - 6\left(\frac{d_{ij}}{dm}\right)^2 + 8\left(\frac{d_{ij}}{dm}\right)^3 - 3\left(\frac{d_{ij}}{dm}\right)^4, & d_{ij} \le dm \\ 0, & d_{ij} > dm \end{cases}, \tag{10}$$

where d_{ij} denotes the distance between (x_i, y_i) and $(x_{i,j}, y_{i,j})$, and dm is the distance between the farthest node and the central node on the star. The weighting function indicates the importance of approximations by Taylor series at different nodes within the star. Namely, the approximation of Tayler series expansion at a node becomes more important if this node is closer to the center of the star. To minimize the above functional with respect to $\mathbf{D_u} = \left\{ \frac{\partial u_i}{\partial x} \; \frac{\partial u_i}{\partial y} \; \frac{\partial^2 u_i}{\partial x^2} \; \frac{\partial^2 u_i}{\partial y^2} \; \frac{\partial^2 u_i}{\partial x \partial y} \right\}^T$ yields a linear equation system:

$$A\mathbf{D_u} = \mathbf{b}, \tag{11}$$

where

$$A = \left\{ \begin{array}{ccccc} \sum\limits_{j=1}^{n_s} h_{ij}^2 w_{ij}^2 & \sum\limits_{j=1}^{n_s} h_{ij}k_{ij}w_{ij}^2 & \sum\limits_{j=1}^{n_s} \frac{h_{ij}^3}{2}w_{ij}^2 & \sum\limits_{j=1}^{n_s} \frac{h_{ij}k_{ij}^2}{2}w_{ij}^2 & \sum\limits_{j=1}^{n_s} h_{ij}^2 k_{ij}w_{ij}^2 \\ & \sum\limits_{j=1}^{n_s} k_{ij}^2 w_{ij}^2 & \sum\limits_{j=1}^{n_s} \frac{h_{ij}^2 k_{ij}}{2}w_{ij}^2 & \sum\limits_{j=1}^{n_s} \frac{k_{ij}^3}{2}w_{ij}^2 & \sum\limits_{j=1}^{n_s} h_{ij}k_{ij}^2 w_{ij}^2 \\ & & \sum\limits_{j=1}^{n_s} \frac{h_{ij}^4}{4}w_{ij}^2 & \sum\limits_{j=1}^{n_s} \frac{h_{ij}^2 k_{ij}^2}{4}w_{ij}^2 & \sum\limits_{j=1}^{n_s} \frac{h_{ij}^3 k_{ij}}{2}w_{ij}^2 \\ & SYM & & \sum\limits_{j=1}^{n_s} \frac{k_{ij}^4}{4}w_{ij}^2 & \sum\limits_{j=1}^{n_s} \frac{h_{ij}k_{ij}^3}{2}w_{ij}^2 \\ & & & & \sum\limits_{j=1}^{n_s} h_{ij}^2 k_{ij}^2 w_{ij}^2 \end{array} \right\}, \tag{12}$$

and

$$\mathbf{b} = \left\{ \begin{array}{c} \sum\limits_{j=1}^{n_s} (-u_i + u_{ij}) h_{ij} w_{ij}^2 \\ \sum\limits_{j=1}^{n_s} (-u_i + u_{ij}) k_{ij} w_{ij}^2 \\ \sum\limits_{j=1}^{n_s} (-u_i + u_{ij}) \frac{h_{ij}^2}{2} w_{ij}^2 \\ \sum\limits_{j=1}^{n_s} (-u_i + u_{ij}) \frac{k_{ij}^2}{2} w_{ij}^2 \\ \sum\limits_{j=1}^{n_s} (-u_i + u_{ij}) h_{ij} k_{ij} w_{ij}^2 \end{array} \right\}. \tag{13}$$

The superscript T denotes the transpose of matrix.

The coefficient matrix $\mathbf{A}$ is clearly symmetric. The explicit expressions for vector $\mathbf{D_u}$ depend on the spatial coordinates of the nodes, the number of nodes in the star, and the choice of weighting function. To decompose the vector $\mathbf{b}$, we have

$$\mathbf{b} = \mathbf{BQ}, \tag{14}$$

where $\mathbf{Q} = [\; u_i \quad u_{i,1} \quad u_{i,2} \quad u_{i,3} \quad \ldots \quad u_{i,n_s} \;]^T$ are the function values at the central node and the other nodes inside the star. Thus, $\mathbf{D_u}$ can be expressed by the following equation:

$$\mathbf{D_u} = \begin{bmatrix} \frac{\partial u_i}{\partial x} \\ \frac{\partial u_i}{\partial y} \\ \frac{\partial^2 u_i}{\partial x^2} \\ \frac{\partial^2 u_i}{\partial y^2} \\ \frac{\partial^2 u_i}{\partial x \partial y} \end{bmatrix} = \mathbf{A}^{-1}\mathbf{b} = \mathbf{A}^{-1}\mathbf{BQ} = \mathbf{A}^{-1}\mathbf{B} \begin{bmatrix} u_i \\ u_{i,1} \\ u_{i,2} \\ u_{i,3} \\ . \\ . \\ . \\ u_{i,n_s} \end{bmatrix}. \tag{15}$$

According to the above expressions, the partial derivatives at the central node can be expressed by linear combinations of the $n_s + 1$ approximate values at the nodes of star. The above system of equations can be written as follows:

$$\left. \frac{\partial u}{\partial x} \right|_i = wx_{i,0} u_i + \sum_{j=1}^{n_s} wx_{i,j} u_{i,j}, \tag{16}$$

$$\left. \frac{\partial u}{\partial y} \right|_i = wy_{i,0} u_i + \sum_{j=1}^{n_s} wy_{i,j} u_{i,j}, \tag{17}$$

$$\left. \frac{\partial^2 u}{\partial x^2} \right|_i = wxx_{i,0} u_i + \sum_{j=1}^{n_s} wxx_{i,j} u_{i,j}, \tag{18}$$

$$\left. \frac{\partial^2 u}{\partial y^2} \right|_i = wyy_{i,0} u_i + \sum_{j=1}^{n_s} wyy_{i,j} u_{i,j}, \tag{19}$$

$$\left. \frac{\partial^2 u}{\partial x \partial y} \right|_i = wxy_{i,0} u_i + \sum_{j=1}^{n_s} wxy_{i,j} u_{i,j}, \tag{20}$$

where $\{wx_{i,j}\}_{j=0}^{n_s}$, $\{wy_{i,j}\}_{j=0}^{n_s}$, $\{wxx_{i,j}\}_{j=0}^{n_s}$, $\{wyy_{i,j}\}_{j=0}^{n_s}$ and $\{wxy_{i,j}\}_{j=0}^{n_s}$ are weighting coefficients corresponding to the ith node and can be calculated numerically.

These expressions and the numerical procedure for obtaining them are the same as those used in [Benito, Urena and Gavete (2001); Chan, Fan and Kuo (2013); Fan, Huang, Li and Chiu (2014)]. These procedures were implemented at every node inside computational domain and along boundary.

We used the governing equations of the Henry problem with given Dirichlet boundary conditions for streamfunction and concentration as an example to illustrate the following numerical procedures. n_i interior nodes and n_b boundary nodes are distributed inside the computational domain and along the boundary. The types of boundary conditions in this illustration are different from the Henry problem for the sake of simplicity. To enforce satisfactions of governing equations, Eqs. (5)-(6), at every interior nodes yields the following system of nonlinear algebraic equations:

$$
\begin{aligned}
F_i^{\psi} =& wxx_{i,0}\psi_i^{n+1} + \sum_{j=1}^{n_s} wxx_{i,j}\psi_{i,j}^{n+1} + wyy_{i,0}\psi_i^{n+1} + \sum_{j=1}^{n_s} wyy_{i,j}\psi_{i,j}^{n+1} \\
& - \frac{1}{a}\left(wx_{i,0}c_i^{n+1} + \sum_{j=1}^{n_s} wx_{i,j}c_{i,j}^{n+1} \right) = 0 \qquad i = 1,2,3,....,n_i,
\end{aligned}
\tag{21}
$$

$$
\begin{aligned}
F_i^c =& wxx_{i,0}c_i^{n+1} + \sum_{j=1}^{n_s} wxx_{i,j}c_{i,j}^{n+1} + wyy_{i,0}c_i^{n+1} + \sum_{j=1}^{n_s} wyy_{i,j}c_{i,j}^{n+1} \\
& - \frac{1}{b}\left(wy_{i,0}\psi_i^{n+1} + \sum_{j=1}^{n_s} wy_{i,j}\psi_{i,j}^{n+1} \right)\left(wx_{i,0}c_i^{n+1} + \sum_{j=1}^{n_s} wx_{i,j}c_{i,j}^{n+1} \right) \\
& + \frac{1}{b}\left(wx_{i,0}\psi_i^{n+1} + \sum_{j=1}^{n_s} wx_{i,j}\psi_{i,j}^{n+1} \right)\left(wy_{i,0}c_i^{n+1} + \sum_{j=1}^{n_s} wy_{i,j}c_{i,j}^{n+1} \right) \\
& - \frac{c_i^{n+1} - c_i^n}{\Delta t} = 0 \qquad i = 1,2,3,....,n_i.
\end{aligned}
\tag{22}
$$

In addition, to enforce the satisfactions of Dirichlet boundary conditions at every boundary nodes will yield another system of algebraic equations:

$$
F_{i+n_i}^{\psi} = \psi_i^{n+1} - \bar{\psi}_i^{n+1} = 0 \quad i = 1,2,3,....,n_b \;\;,
\tag{23}
$$

$$
F_{i+n_i}^c = c_i^{n+1} - \bar{c}_i^{n+1} = 0 \quad i = 1,2,3,....,n_b \;\;,
\tag{24}
$$

where $\bar{\psi}_i^{n+1}$ and $\bar{c}_i^{n+1}$ are prescribed boundary conditions for streamfunction and concentration at the ith node and in the $(n+1)^{th}$ time step. Once the GFDM and the implicit Euler method were adopted for spatial and temporal discretizations, a system of $2 \times (n_i + n_b)$ non-linear algebraic equations with $2 \times (n_i + n_b)$ unknowns, Eqs. (21)-(24), was yielded. We used

$$
\mathbf{F} = \left[F_1^{\psi}, F_2^{\psi}, F_3^{\psi}, ..., F_{n_i+n_b}^{\psi}, F_1^c, F_2^c, F_3^c, ..., F_{n_i+n_b}^c \right]^T
$$

and

$$\mathbf{q} = \left[\psi_1^{n+1}, \psi_2^{n+1}, \psi_3^{n+1}, \ldots\ldots, \psi_{n_i+n_b}^{n+1}, c_1^{n+1}, c_2^{n+1}, c_3^{n+1}, \ldots\ldots, c_{n_i+n_b}^{n+1} \right]^T$$

to denote the equations and unknowns of the above system. Then, the Newton-Raphson method, described in the following subsection, was adopted to efficiently solve the resultant system of non-linear algebraic equations.

3.3   Newton-Raphson method

When the Newton-Raphson method is adopted for iteratively solving the above system of non-linear algebraic equations, the iterative formula is expressed as,

$$\mathbf{q}^{k+1} = \mathbf{q}^k - \left(\mathbf{B}^k\right)^{-1} \mathbf{F}^k \quad k = 0, 1, 2, 3, \ldots\ldots\ldots \quad , \tag{25}$$

where the superscripts $k+1$ and k denote the $(k+1)^{th}$ and the kth iterative steps, respectively. The superscript -1 denotes the inverse of matrix and $\mathbf{B}$ is the Jacobian matrix with its component $B_{ij} = \frac{\partial F_i}{\partial q_j}$. The solutions of streamfunction and salt concentration at the nth time step were used as the initial guess of the Newton-Raphson method $(k=0)$. Since the computation for inverse of Jacobian matrix in Eq. (25) is extremely time-consuming, especially for large-scale systems, the iteration process in Eq. (25) is split into two sequent steps,

$$\mathbf{B}^k \left(\mathbf{q}^{k+1} - \mathbf{q}^k \right) = \mathbf{B}^k \Delta \mathbf{q}^k = -\mathbf{F}^k, \tag{26}$$

$$\mathbf{q}^{k+1} = \mathbf{q}^k + \Delta \mathbf{q}^k. \tag{27}$$

Because the Jacobian matrix from the GFDM and the implicit Euler method is sparse, the system of linear algebraic equations in Eq. (26) can be solved by any efficient iterative solvers, such as the conjugate gradient method. Once the sparse system of Eq. (26) is solved, the solutions at the $(k+1)^{th}$ iterative step can be acquired by using Eq. (27). The stopping criteria for iteration of the Newton-Raphson method is expressed as follows,

$$\underset{j}{Max} \left| \mathbf{q}_j^{k+1} - \mathbf{q}_j^k \right| \le \varepsilon, \tag{28}$$

where ε is a pre-defined parameter and $\varepsilon = 10^{-9}$ is adopted for all tests in this paper. While the iteration process reaches the stopping criteria, Eq. (28), the iteration process can be terminated and then the convergent solutions for streamfunction and concentration at the $(n+1)^{th}$ time step were acquired. The solution procedures are repeated until the steady state or the terminal time is reached.

4   Numerical results and comparisons

In this section, we adopted the proposed numerical scheme, a combination of the GFDM, the implicit Euler method and the Newton-Raphson method, to analyze the problems of density-driven groundwater flows. The Henry and the Elder problems are two benchmark tests and they are analyzed by the proposed meshless methods. In addition, several factors in the proposed numerical method were systematically examined by a series of numerical experiments. The numerical results were compared with other numerical and semi-analytical solutions.

4.1   *Henry problem*

The first example in this paper is the Henry problem. The schematic diagram of the Henry problem, which includes the computational domain Ω and boundary conditions, is depicted in Fig. 1(a). Besides, the interior nodes and the boundary nodes are uniformly distributed inside the domain and along the boundary $\partial\Omega$, that are demonstrated in Fig. 1(b). From previous studies [Simpson and Clement (2004); Soto Meca, Alhama and Gonzalez Fernandez (2007)], there are three different versions of the Henry problems according to the parameters, *a* and *b*, in the governing equations. The problem is known as the original Henry saltwater intrusion problem for *a*=0.2637 and *b*=0.1, while it is called the Pinder version of Henry problem for *a*=0.2637 and *b*=0.035. The third version is denoted as the modified Henry problem if *a*=0.1315 and *b*=0.2 are adopted. We analyzed these three versions of Henry problem by the proposed method in the subsection.

In the following tests, these parameters are used: $N = 3317$ (number of total nodes), $\Delta t = 0.001$ (time increment) and $n_s = 16$ (number of nodes in a star). First, the original Henry saltwater intrusion problem (*a*=0.2637 and *b*=0.1) is simulated by the proposed method and the results are demonstrated in Figs. 3 and 4. The distributions of streamlines and salt concentration at different specific time are depicted in Figs. 3(a)-3(e) and Figs. 4(a)-4(e). The movements of salt concentration can be obviously observed in these figures since the computational domain is initially filled with freshwater. In addition, we plotted the distribution of steady-state velocity vector in Fig. 5 and the flow field of this problem is very clear. Inside the aquifer, there is a mainstream from left to right due to the movement of freshwater. On the other hand, in the right bottom corner, there is a small circulation due to the salt concentration form seaside boundary. The steady-state solutions of streamlines and concentration in Figs. 3(e) and 4(e) are compared well with results by the local boundary integral equation method [Kovarik and Muzik (2013)] and by the network simulation method [Soto Meca, Alhama and Gonzalez Fernandez (2007)].

In order to examine the consistency of the proposed method, four different numbers
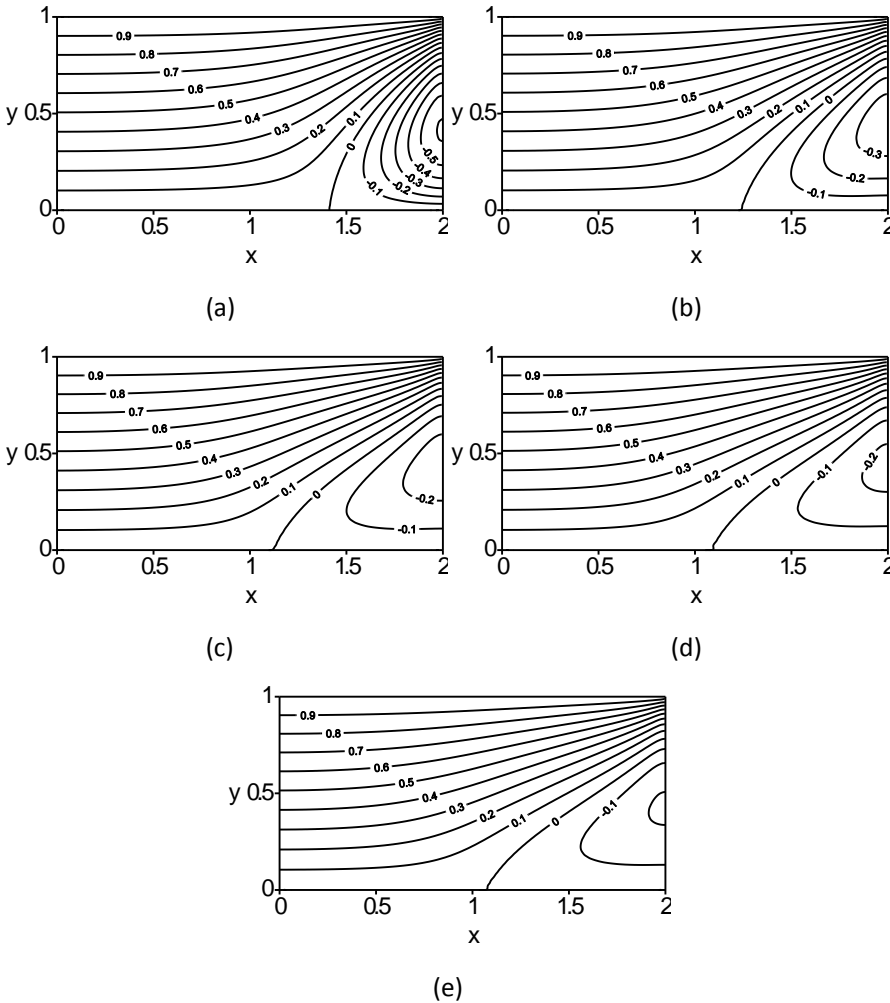
Figure 3: Distributions of streamlines at different specific time for Henry problem, (a) t=0.02, (b) t=0.05, (c) t=0.10, (d) t=0.15 and (e) steady-state (t=0.21). (a=0.2637, b=0.1, 3317 nodes).

of nodes are adopted in this test. The steady-state solutions of streamlines and salt concentration by using 227, 857, 3317 and 5147 nodes are shown in Figs. 6 and 7. Although there are some small differences of the solutions by using 227 and 857 nodes from the other two solutions, the solutions by using 227 and 857 nodes still can correctly acquire the most part of the distributions of streamlines and salt concentration. From these two figures, the consistency of the proposed method can
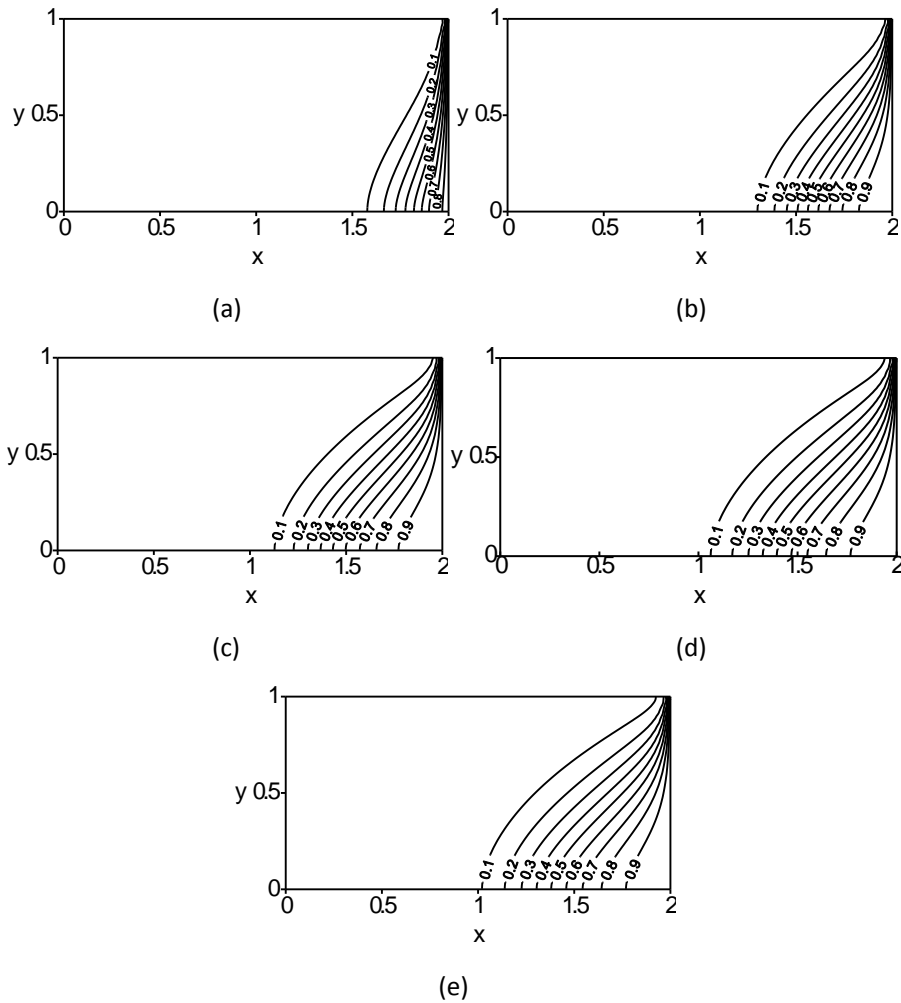
Figure 4: Distributions of salt concentration at different specific time for Henry problem, (a)t=0.02, (b) t=0.05, (c) t=0.1, (d) t=0.15 and (e) steady-state (t=0.21). (a=0.2637, b=0.1, 3317 nodes).

be verified and the solutions can be acquired by adopting very few nodes. When 5147 nodes are adopted, in every time step we will have a system of 10294 non-linear algebraic equations with 10294 unknowns. Because the Jacobian matrix from the GFDM is sparse, this case still can be efficiently solved. In order to check the influence of the number of nodes in a star on the numerical accuracy, the profiles of isochlor c=0.5 are depicted in Fig. 8. The solutions by using n_s=12, 16 and
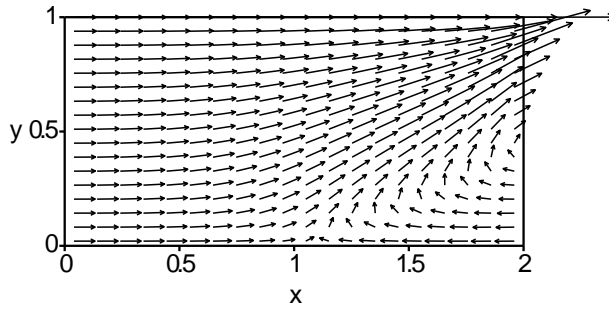
Figure 5: Distribution of velocity vectors for the Henry problem (*a*=0.2637, *b*=0.1).
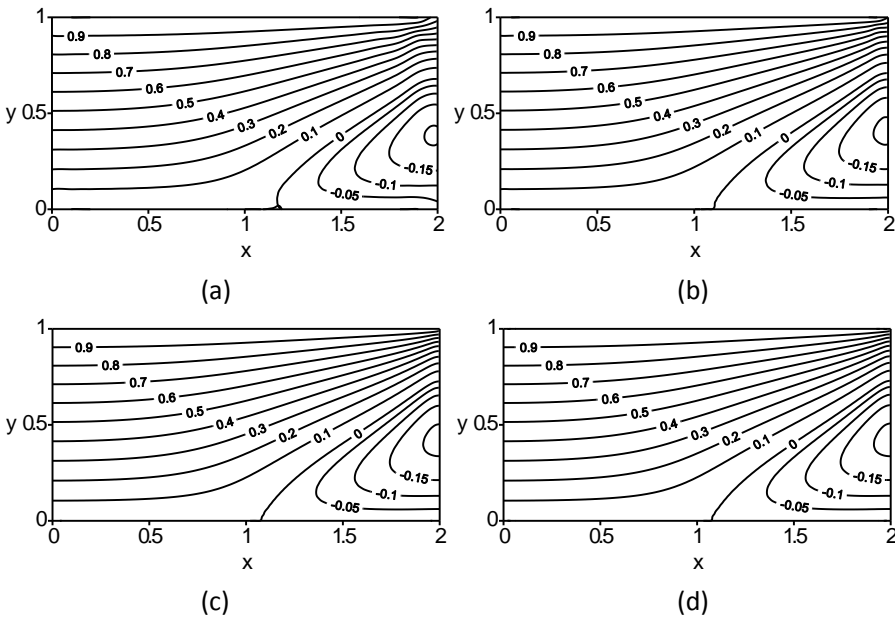
Figure 6: The steady-state solutions of streamlines for Henry problem by using different numbers of nodes. (a) 227 nodes, (b) 857 nodes, (c) 3317 nodes and (d) 5147 nodes. (*a*=0.2637, *b*=0.1).
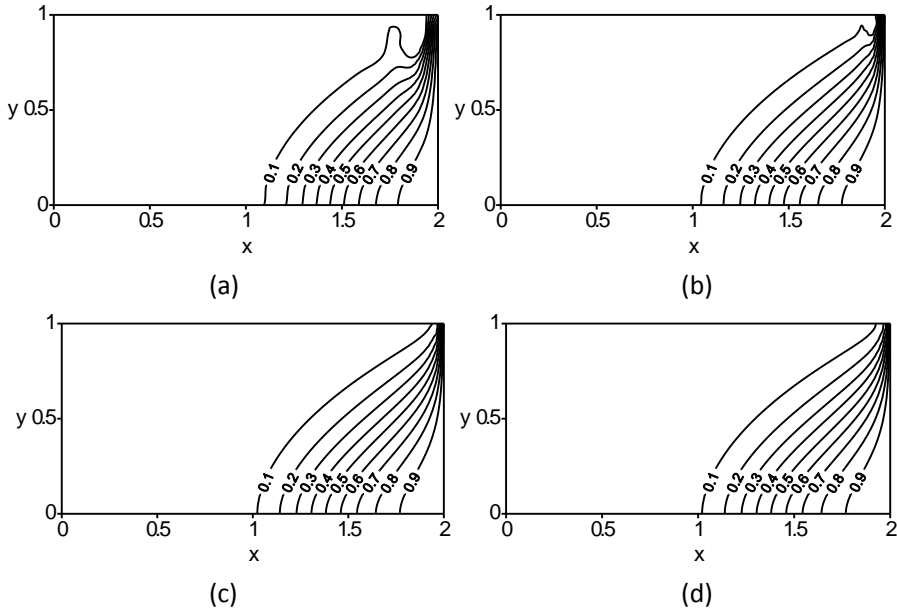
Figure 7: The steady-state solutions of salt concentration for Henry problem by using different numbers of nodes. (a) 227 nodes, (b) 857 nodes, (c) 3317 nodes and (d) 5147 nodes. (a=0.2637, b=0.1).

20 are almost identical to each other and they are very similar with other solutions [Kovarik and Muzik (2013); Soto Meca, Alhama and Gonzalez Fernandez (2007)]. Thus, from these comparisons, it is validated that the proposed numerical scheme is very stable with respect to the number of total nodes and the number of nodes in a star.

After the validations from previous test, the Pinder version of Henry problem (a=0.2637, b=0.035) is solved by the proposed meshless method. The numerical solutions of the Pinder version of Henry problem by using different numbers of nodes are demonstrated in Figs. 9 and 10. Though, the distributions of streamlines and salt concentration by using 227 and 857 nodes show little difference from the other two solutions, they still can provide the acceptable solutions in most part of the computational domain. Besides, the solutions obtained by using 3317 and 5147 nodes are almost identical to other numerical solutions [Kovarik and Muzik (2013); Soto Meca, Alhama and Gonzalez Fernandez (2007)]. The distribution of velocity vector is shown in Fig. 11 and a stagnation point near the center of bottom boundary can be easily found. By comparing Fig. 5 with Fig. 11, we can find that the
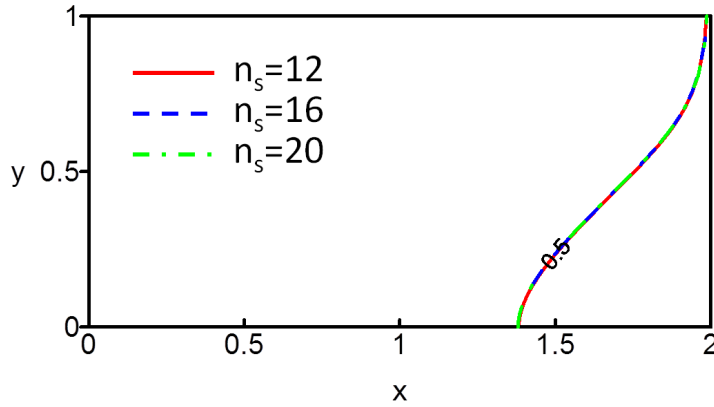
Figure 8: Profiles of isochlor $c=0.5$ for Henry problem by using different numbers of nodes in star. ($a=0.2637$, $b=0.1$).

(a)

(b)

(c)

(d)
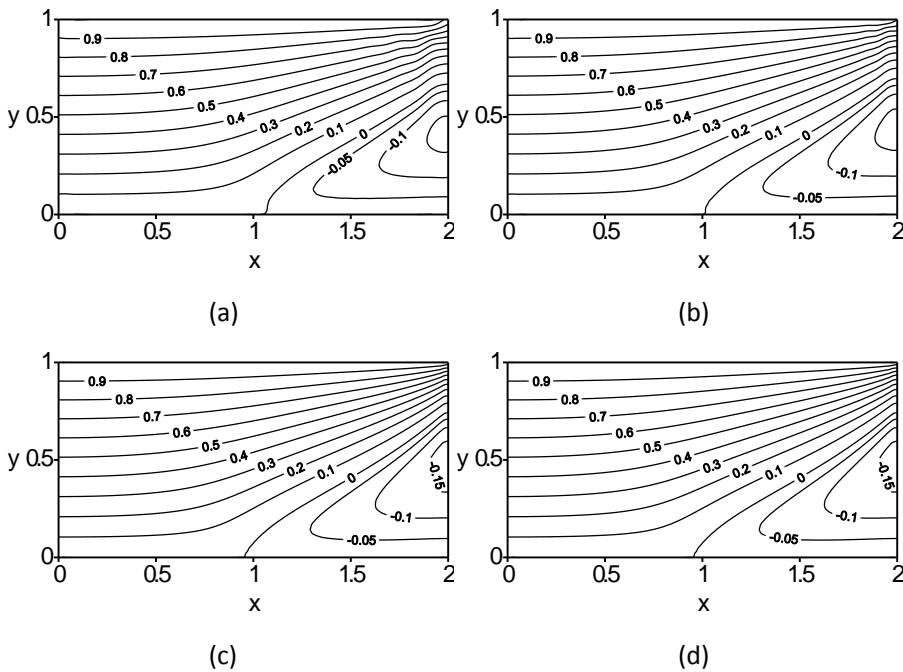
Figure 9: The steady-state solutions of streamlines for the Pinder version of Henry problem by using different numbers of nodes. (a) 227 nodes, (b) 857 nodes, (c) 3317 nodes and (d) 5147 nodes. ($a=0.2637$, $b=0.035$).
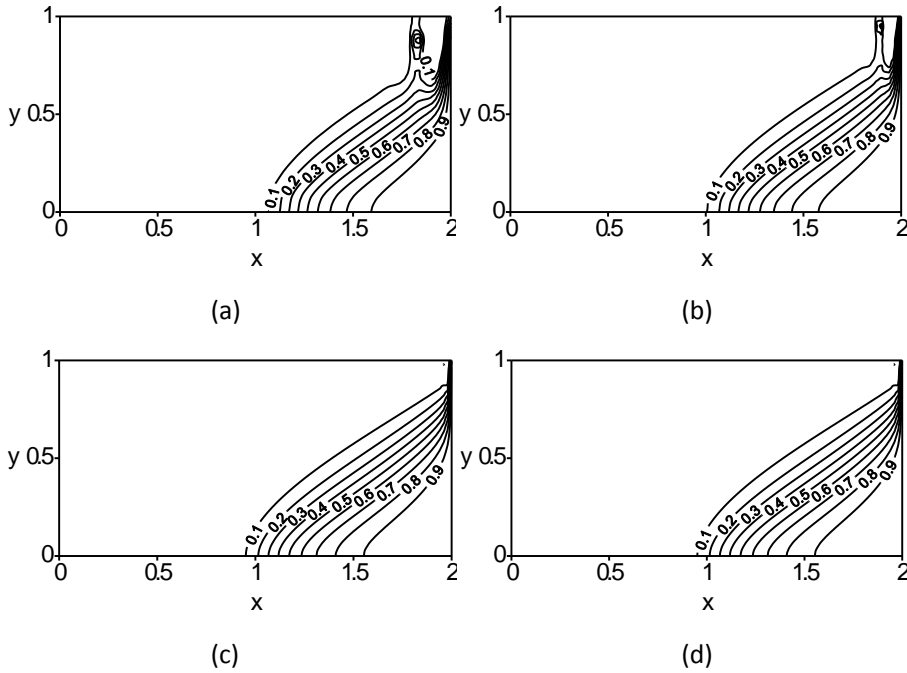
Figure 10: The steady-state solutions of salt concentration for the Pinder version of Henry problem by using different numbers of nodes. (a) 227 nodes, (b) 857 nodes, (c) 3317 nodes and (d) 5147 nodes. (a=0.2637, b=0.035).
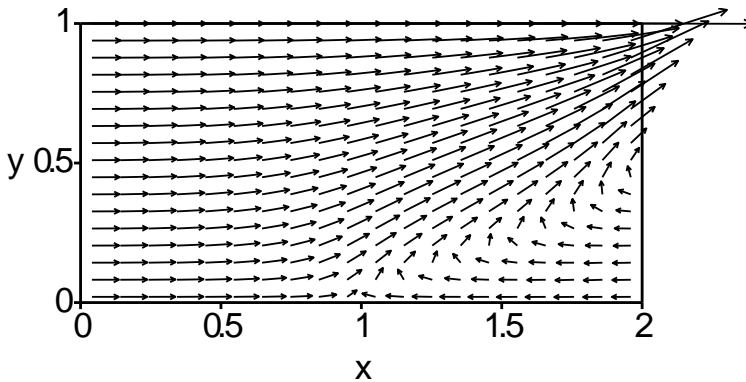
Figure 11: Distribution of velocity vectors for the Pinder version of Henry problem. (a=0.2637, b=0.035).
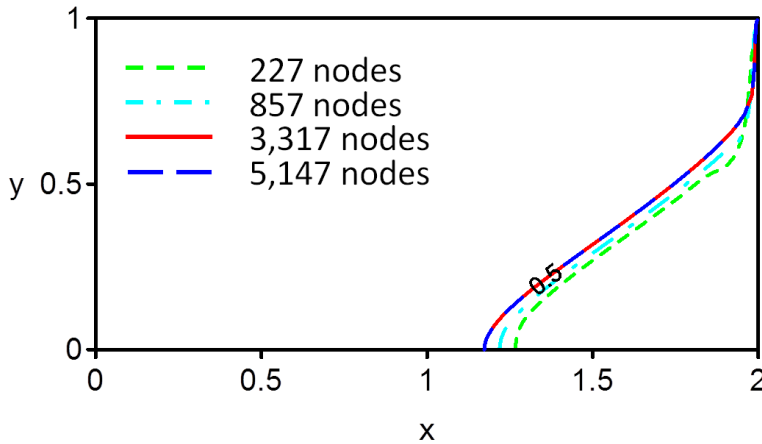
Figure 12: Profiles of isochlor $c=0.5$ for the Pinder version of Henry problem by using different numbers of total nodes. ($a=0.2637$, $b=0.035$).

problem of saltwater intrusion in the Pinder version of Henry problem ($a=0.2637$, $b=0.035$) becomes worse than the original Henry problem ($a=0.2637$, $b=0.1$). The profiles of the isochlor $c=0.5$ are depicted in Fig. 12. From this figure, the consistency of the proposed method can be verified. Namely, the numerical solutions are stably convergent when the number of nodes becomes larger and larger.

The third test in this examples is known as the modified Henry problem ($a=0.1315$, $b=0.2$). The steady-state distributions of streamlines and salt concentration are illustrated in Fig. 13 and are compared well with results from Soto Meca, Alhama and Gonzalez Fernandez (2007). Besides, the distribution of velocity vector is shown in Fig. 14. The circulation in the right bottom corner becomes larger when the solutions are compared with the previous two tests of Henry problem, which means the problem of saltwater intrusion is the worst among them. In this test, we used different time increments to show the stability of the proposed method. The profiles of the isochlor $c=0.5$ by adopting different time increments ($\Delta t=0.1$, 0.01, 0.001) are demonstrated in Fig. 15 and these provided solutions are almost identical to each other, which demonstrates the good stability of the proposed method.

The positions of the x-Toe of the isochlor $c=0.5$ by using different numbers of total nodes are tabulated in Table 1. The consistency of the proposed method and the influence of the parameters, a and b, can be easily observed. In addition, the positions of the x-Toe of the isochlor $c=0.5$ are well compared with other results [Gotovac, Andricevic, Gotovac, Kozulic and Vranjes (2003); Henry (1964); Langevin and Guo (1999); Pinder and Cooper Jr. (1970); Segol, Pinder, Gray (1975); Simpson
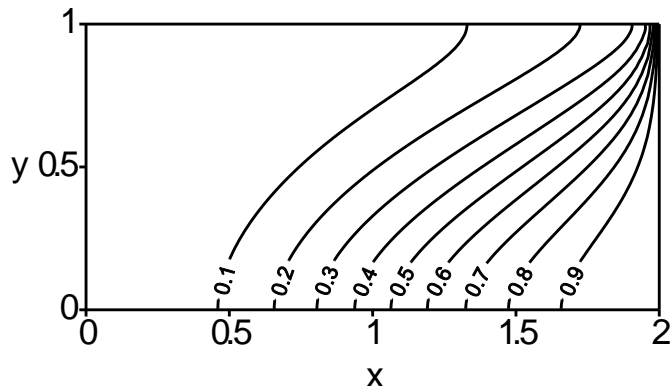
(a)
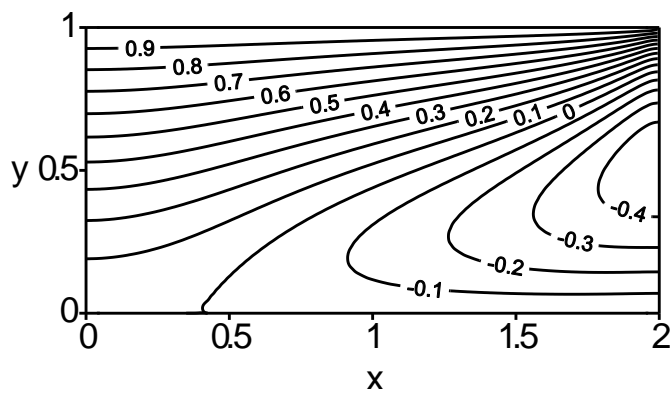
(b)

Figure 13: Distributions of the steady-state solutions of (a) concentration and (b) streamlines for modified Henry problem. (a=0.1315, b=0.2, 3317 nodes).
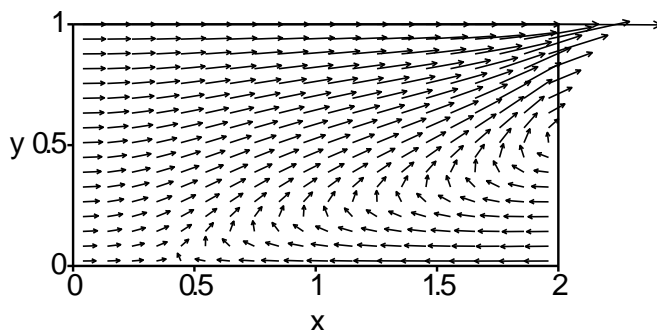
Figure 14: Distribution of velocity vectors for the modified Henry problem. (a=0.1315, b=0.2).
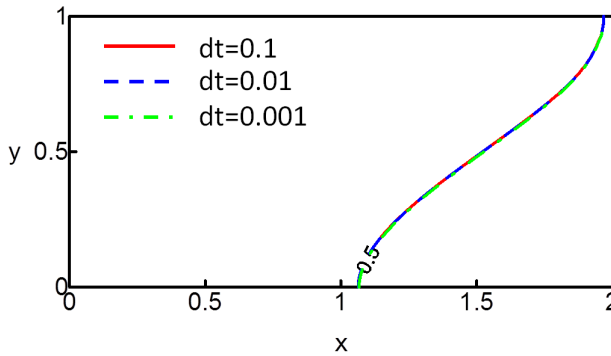
Figure 15: Profiles of isochlor c=0.5 for the modified Henry problem by using different time increments. (a=0.1315, b=0.2).

Table 1: The x-Toe positions of isochlor c=0.5 by using different numbers of total nodes for the Henry problem.

Number of nodes	Toe shoe a=0.2637, b=0.1	Toe shoe a=0.2637, b=0.035	Toe shoe a=0.1315, b=0.2
227	1.4383	1.3071	1.1099
857	1.3973	1.2691	1.0751
3,317	1.3982	1.1799	1.0636
5,147	1.3802	1.1729	1.0560

and Clement (2004); Soto Meca, Alhama and Gonzalez Fernandez (2007)] in Table 2. The data of other researches in Table 2 are acquired from Soto Meca, Alhama and Gonzalez Fernandez (2007). Although the solutions from different study in Table 2 show a little difference from each other, it can be noticed that the numerical results acquired by our method are very close to those in recently-published papers [Gotovac, Andricevic, Gotovac, Kozulic and Vranjes (2003); Simpson and Clement (2004); Soto Meca, Alhama and Gonzalez Fernandez (2007)]. It is quite reasonable that the solutions in recently-published papers are more reliable than those, published in three decades ago, since computer technology and numerical methods have been rapidly developed in the past decades. Hence, it can be concluded that these numerical results by using the proposed method are consistent with other studies in this table. Consequently, the accuracy of the proposed method is verified by comparing these numerical results with other solutions. In addition, the stability, the consistency and the simplicity of the proposed scheme are validated by the provided results for the three versions of the Henry problem.

Table 2: Comparisons of the x-Toe positions of isochlor *c*= 0.5 by the proposed method with other solutions.

a=0.2637,*b*=0.1	*a*=0.2637,*b*=0.035	*a*=0.1315,*b*=0.2
1.089 [Henry, 1964]	1.220 [Pinder and Cooper, 1970]	1.074 [Langevin and Guo, 1999]
1.371 [Gotovac et al., 2003]	1.245 [Segol et al., 1975]	1.078 [Simpson and Clement, 2004, (Semi-analytical solution)]
1.393 [Simpson and Clement, 2004, (Semi-analytical solution)]	1.154 [Gotovac et al., 2003]	1.074 [Simpson and Clement, 2004, (Numerical solution)]
1.373 [Soto Meca et al., 2007]	1.158 [Soto Meca et al., 2007]	1.059 [Soto Meca et al., 2007]
1.380 Present study (5,147 nodes)	1.173 Present study (5,147 nodes)	1.056 Present study (5,147 nodes)

4.2 Elder problem

The second example in this paper is the Elder problem. In this test, the Rayleigh number *Ra* is set as 400 and other parameters are: $N = 6597$, $\Delta t = 0.001$ and $n_s = 16$. The schematic diagram, the computational domain and the boundary conditions of the Elder problem are illustrated in Fig 2(a). Besides, the interior nodes and the boundary nodes are uniformly distributed inside the domain and along the boundary, which are shown in Fig 2(b). Since the aspect ratio of computational domain in the Elder problem is larger than that in the Henry problem, we adopted more nodes to analyze the Elder problem. The computational domain and the boundary conditions are symmetric with respect to a vertical axis at *x*=2, such that only solutions in left half domain are demonstrated for the sake of simplicity. The steady-state solutions of concentration, streamlines and velocity vector are shown in Fig 16. From Fig. 16(c), two main circulations moving in different directions can be obviously observed. Besides, the salt concentration from the upper source moved toward the bottom also can be found in Fig. 16(a).

The distributions of streamlines and salt concentration at different specific time are depicted in Figs. 17 and 18. From these two figures, the variations of the flow fields and salt concentration at several different specific time are apparent. The steady-state solutions also agreed well with other solutions [Soto Meca, Alhama

and Gonzalez Fernandez (2007)]. In order to verify the consistency of the proposed scheme, the numerical results by using 447, 1697, 4552 and 6597 nodes are depicted in Fig. 19. The numerical results are quite stable if more nodes are used. From the numerical experiments in this example, the accuracy and the consistency of the proposed method are verified by these comparisons.
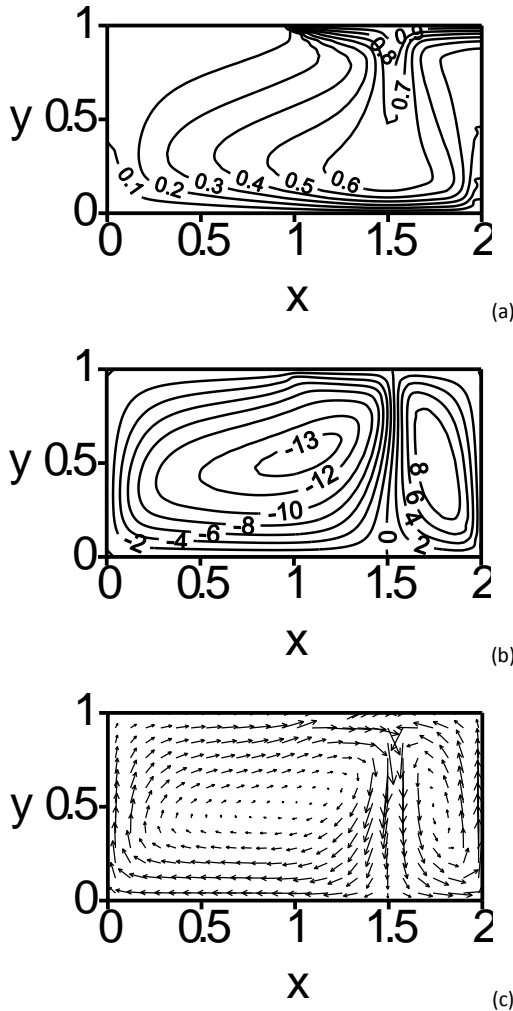
Figure 16: Distributions of steady-state solutions for (a) concentration, (b) streamlines and (c) velocity vectors for the Elder problem (6597 nodes).
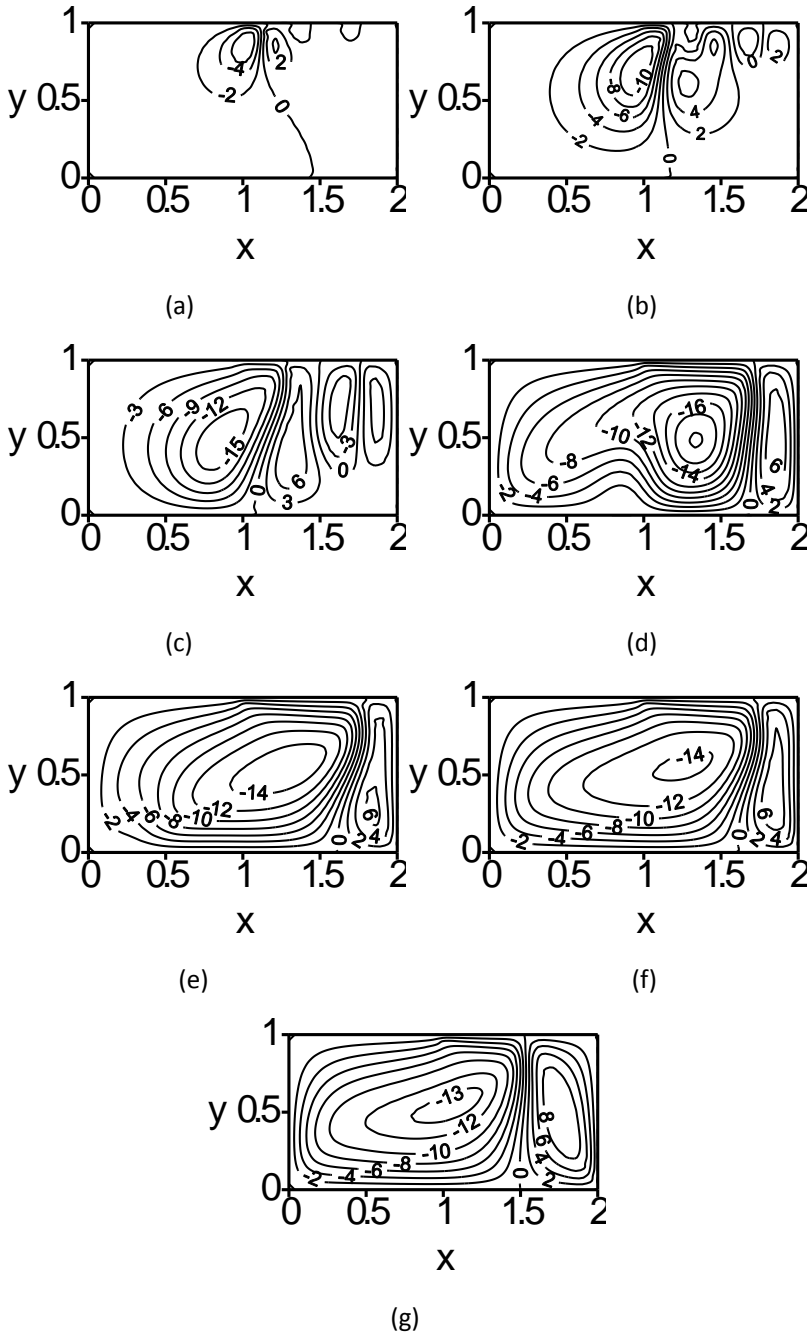
Figure 17: Distributions of streamlines at different specific time for Elder problem, (a) t=0.005, (b) t=0.01, (c) t=0.02, (d) t=0.05, (e) t=0.075, (f) t=0.1 and (g) steady-state (t=1.239). (6597 nodes)
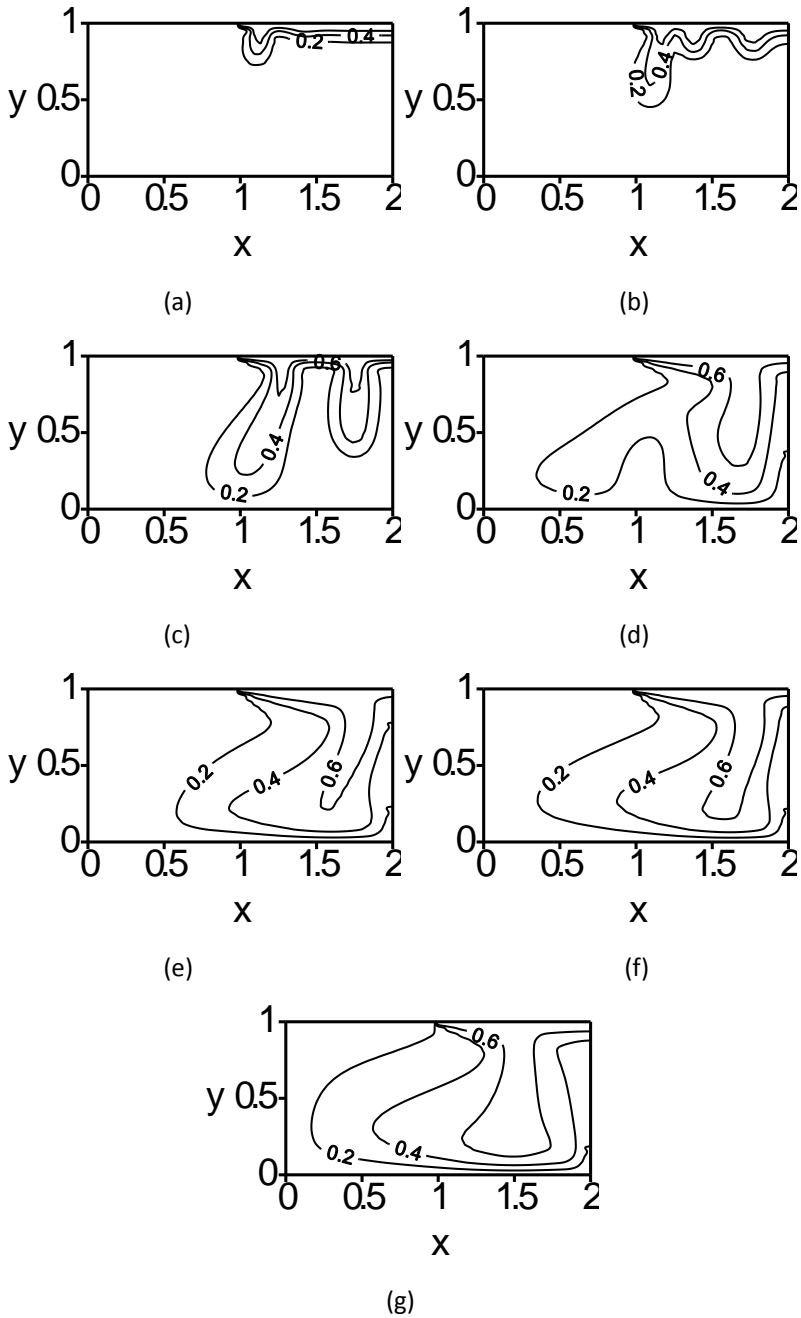
Figure 18: Distributions of salt concentration at different specific time for Elder problem, (a) *t*=0.005, (b) *t*=0.01, (c) *t*=0.02, (d) *t*=0.05, (e) *t*=0.075, (f) *t*=0.1 and (g) steady-state (*t*=1.239). (6597 nodes)
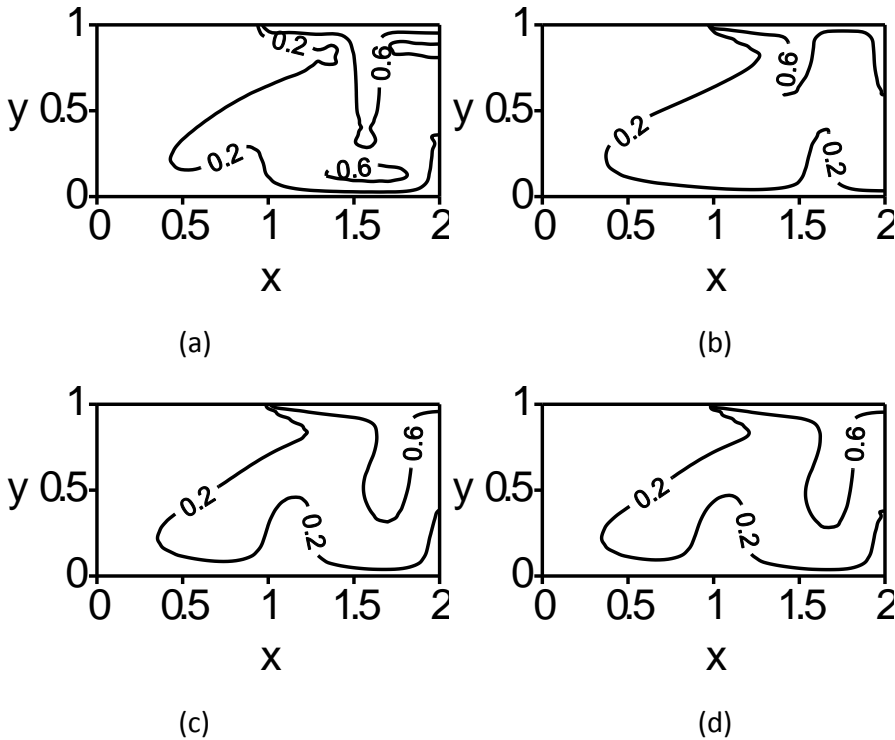
Figure 19: Profiles of the isochlors $c=0.2$ and $c=0.6$ for Elder problem at $t=0.05$ by using different numbers of total nodes. (a) 447 nodes, (b) 1697 nodes, (c) 4552 nodes and (d) 6597 nodes.

5   Conclusions

A combination of the GFDM, the implicit Euler method and the Newton-Raphson method is proposed to analyze the problems of density-driven groundwater flows. It is of great importance to develop a reliable and efficient numerical model for these problems, since density-driven groundwater flows are related to problems of saltwater intrusion and geothermal processes as well as their governing equations are very complicated. In the proposed numerical scheme, the GFDM, one of the most promising meshless methods, and the implicit Euler method were adopted for spatial and temporal discretizations. After these discretizations, a system of nonlinear algebraic equations at every time step is yielded and then is solved by the Newton-Raphson method. Because the Jacobian matrix from the GFDM and the implicit Euler method is sparse, the iteration process in the Newton-Raphson method can be efficiently calculated.

The Henry and the Elder problems are two benchmark problems of the density-driven groundwater flows, such that we used these two examples to verify the accuracy and the stability of the proposed method. We successfully investigated three different versions of the Henry problem, which include the original Henry saltwater intrusion problem, the Pinder version of Henry problem and the modified Henry problem. The numerical solutions of the Henry and the Elder problems agreed well with other results. In addition, solutions by using different numbers of total nodes, different numbers of nodes in a star and different time increments are provided to validate the merits of the proposed meshless method. The proposed approach can be directly extended to three-dimensional saltwater intrusion problems or realistic engineering problems in the near future.

References

Benito, J. J.; Urena, F.; Gavete, L. (2001): Influence of several factors in the generalized finite difference method. *Applied Mathematical Modelling,* vol. 25, pp. 1039-1053.

Benito, J. J.; Urena, F.; Gavete, L. (2007): Solving parabolic and hyperbolic equations by the generalized finite difference method. *Journal of Computational and Applied Mathematics,* vol. 209, pp. 208-233.

Benito, J. J.; Urena, F.; Gavete, L.; Alonso, B. (2008): Application of the generalized finite difference method to improve the approximated solution of pdes. *Computer Modeling in Engineering & Sciences,* vol. 38, no. 1, pp. 39-58.

Chan, H. F.; Fan, C. M.; Kuo, C. W. (2013): Generalized finite difference method for solving two-dimensional nonlinear obstacle problem. *Engineering Analysis with Boundary Elements,* vol. 37, pp. 1189-1196.

Chan, H. F.; Fan, C. M. (2013): The local radial basis function collocation method for solving two-dimensional inverse Cauchy problems. *Numerical Heat Transfer, Part B*, vol. 63, pp. 284-303.

Chen, C. S.; Fan, C. M.; Wen, P. H. (2011): The method of approximate particular solutions for solving elliptic problems with variable coefficients. *International Journal of Computational Methods*, vol. 8, no. 3, pp. 545-559.

Chen, C. S.; Fan, C. M.; Wen, P. H. (2012): The method of approximate particular solutions for solving certain partial differential equations. *Numerical Methods for Partial Differential Equations*, vol. 28, pp. 505-522.

Chen, W.; Fu, Z.; Wei, X. (2009): Potential problems by singular boundary method satisfying moment condition. *Computer Modeling in Engineering & Sciences,* vol. 54, no. 1, pp. 65-85.

Elder, J. W. (1967): Transient convection in a porous medium, *Journal of Fluid Mechanics*, vol. 27, pp. 609–723.

Fan, C. M.; Chien, C. S.; Chan, H. F.; Chiu C. L. (2013): The local RBF collocation method for solving the double-diffusive natural convection in fluid-saturated porous media *International Journal of Heat and Mass Transfer*, vol. 57, pp. 500-503.

Fan, C. M.; Huang, Y. K.; Li, P. W.; Chiu, C. L. (2014): Application of the generalized finite-difference method to inverse biharmonic boundary-value problems. *Numerical Heat Transfer, Part B*, vol. 65, pp. 129-154.

Fan, C. M.; Li, H. H.; Hsu, C. Y.; Lin, C. H. (2014): Solving inverse Stokes problems by modified collocation Trefftz method. *Journal of Computational and Applied Mathematics*, vol. 268, pp. 68-81.

Fan, C. M.; Liu, Y. C.; Chan, H. F.; Hsiao S. S. (2014): Solutions of boundary detection problem for modified Helmholtz equation by Trefftz method. *Inverse Problems in Science & Engineering*, vol. 22, no. 2, pp. 267-281.

Fan, C. M.; Liu, C. S.; Yeih, W.; Chan, H. F. (2010): The scalar homotopy algorithm for solving non-linear obstacle problem. *Computers, Materials & Continua*, vol. 15, no. 1, pp. 67-86.

Gaspar, C. (2013): A regularized method of fundamental solutions without desingularization. *Computer Modeling in Engineering & Sciences,* vol. 92, no. 1, pp. 103-121.

Gavete, L.; Urena, F.; Benito, J. J. (2003): Improvements of generalized finite difference method and comparison with other meshless method. *Applied Mathematical Modelling,* vol. 27, pp. 831-847.

Gavete, L.; Urena, F.; Benito, J. J.; Gavete, M. L. (2012): Modelling of the advection–diffusion equation with a meshless method without numerical diffusion. *International Journal of Computer Mathematics,* vol. 89, no. 3, pp. 377-389.

Gotovac, H.; Andricevic, R.; Gotovac, B.; Kozulic, V.; Vranjes, M. (2003): An improved collocation method for solving the Henry problem. *Journal of Contaminant Hydrology*, vol. 64, pp. 129– 149.

Henry H. R. (1964): Effects of dispersion on salt encroachment in coastal aquifers. *Sea Water in Coastal Aquifers, US Geologocal Survey Water Supply Paper 1613-C*, pp. 70–84.

Kovarik, K.; Muzik, J. (2013): A meshless solution for two dimensional density-driven groundwater flow. *Engineering Analysis with Boundary Elements*, vol. 37, pp. 137-196.

Langevin, C. D.; Guo, W. (1999): Improvements to SEAWAT, a variable-density

modeling code. *in Eos, Transactions,* vol. 80, no. 46, pp. F-373.

Lin, J.; Chen, W.; Chen, C. S.; Jiang, X. R. (2013): Fast boundary knot method for solving axisymmetric Helmholtz problems with high wave number. *Computer Modeling in Engineering & Sciences,* vol. 94, no. 6, pp. 485-505.

Liu, C. S.; Atluri, S. N. (2008): A novel time integration method for solving a large system of non-linear algebraic equations. *Computer Modeling in Engineering & Sciences,* vol. 31, pp. 71-83.

Liu, C. S.; Atluri, S. N. (2009): A fictitious time integration method for the numerical solution of the Fredholm integral equation and for numerical differentiation of noisy data, and its relation to the filter theory. *Computer Modeling in Engineering & Sciences,* vol. 41, pp. 243-262.

Liu, Q. G.; Sarler, B. (2013): Non-singular method of fundamental solutions for two-dimensional isotropic elasticity problems. *Computer Modeling in Engineering & Sciences,* vol. 91, no. 4, pp. 235-266.

Mirzaei, D.; Dehghan, M. (2011): MLPG method for transient heat conduction problem with MLS as trial approximation in both time and space domains. *Computer Modelling in Engineering & Sciences,* vol. 72, no. 3, pp. 185-210.

Mramor, K.; Vertnik, R.; Sarler, B. (2013): Low and intermediate Re solution of lid driven cavity problem by local radial basis function collocation method. *Computers, Materials & Continua*, vol. 36, no. 1, pp. 1-21.

Pinder, G. F.; Cooper Jr., H. H. (1970): A numerical technique for calculating the transient position of the saltwater front. *Water Resources Research*, vol. 6, no. 3, pp. 875–882.

Segol, G.; Pinder, G. F.; Gray, W. G. (1975): A Galerkin-finite element technique for calculating the transient position of the saltwater front. *Water Resources Research*, vol. 11, no. 2, pp. 343–347.

Simpson, M. J.; Clement, T. P. (2003): Theoretical analysis of the worthiness of Henry and Elder problems as benchmarks of density-dependent groundwater flow models. *Advances in Water Resource*, vol. 26, pp. 17–31.

Simpson, M. J.; Clement, T. P. (2004): Improving the worthiness of the Henry problem as a benchmark for density-dependent groundwater flow models. *Water Resources Research*, vol. 40, pp. W01504.

Sladek, J.; Sladek, V.; Krahulec, S.; Wunsche, M.; Zhang, Ch. (2012): MLPG analysis of layered composites with piezoelectric and piezomagnetic phases. *Computers, Materials & Continua*, vol. 29, no. 1, pp. 75-101.

Soto Meca, A.; Alhama, F.; Gonzalez Fernandez, C. F. (2007): An efficient model for solving density driven groundwater flow problems based on the network

simulation method. *Journal of Hydrology*, vol. 339, pp. 39–53.

Tsai, C. C.; Young, D. L. (2013): Using the method of fundamental solutions for obtaining exponentially convergent Helmholtz eigensolutions. *Computer Modeling in Engineering & Sciences,* vol. 94, no. 2, pp. 175-205.

Urena, F.; Benito, J. J.; Gavete, L. (2011): Application of the generalized finite difference method to solve the advection–diffusion equation. *Journal of Computational and Applied Mathematics,* vol. 235, pp. 1849-1855.

Zheng, H.; Chen, W.; Zhang, C. (2013): Multi-domain boundary knot method for ultra-thin coating problems. *Computer Modeling in Engineering & Sciences,* vol. 90, no 3, pp. 179-195.